Journal of Materials Chemistry C

Accepted Manuscript

This article can be cited before page numbers have been issued, to do this please use: A. Catellani, A. Ruini and A. Calzolari, *J. Mater. Chem. C*, 2015, DOI: 10.1039/C5TC01699A.

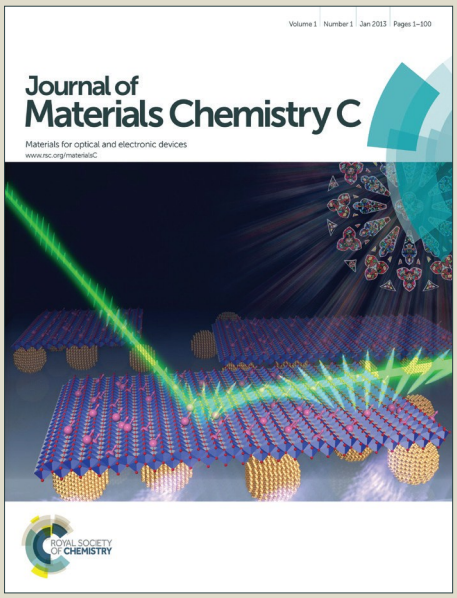

ROYAL SOCIETY OF CHEMISTRY

www.rsc.org/materialsC

ARTICLE TYPE www. rsc.org/xxxxxx | XXXXXXXX DOI: 10.1039/C5TC01699A

Optoelectronic properties and color chemistry of native point defects in Al:ZnO transparent conductive oxide†

Alessandra Catellani,[a,b] **Alice Ruini,**[c,a] **and Arrigo Calzolari**[*a]

Received Xth XXXXXXXXXX 20XX, Accepted Xth XXXXXXXXX 20XX
First published on the web Xth XXXXXXXXXX 200X
DOI: 10.1039/b000000x

We present a first principles study on the effect of native point defects in Al:ZnO transparent conductive oxide. Our results indicate that oxygen and zinc vacancies play two completely different roles: the former maintain the electrical properties while worsening the transparency of native Al:ZnO. The latter are strong electron acceptors that can destroy the metal-like conductivity of the system. While the percentage of doping amount is not really relevant, the compensation ratio between Zn vacancy and Al dopants is crucial for the final electrical properties of the system. H impurities always act as electron donors and generally improve the characteristics of the transparent conductor. Finally, we show how the chemistry of the defects affect the color of Al:ZnO samples, in agreement with experimental results. Our results pave the way to defect engineering for the growth of high performance transparent conductive oxides.

1 Introduction

Transparent conducting oxides (TCOs) are electrical conductive materials with a low absorption of light in the visible range.[1–3] The unique combination of metallicity and transparency makes TCOs appealing for a variety of applications,[4–7] including photovoltaic cells, flat displays, smart windows, invisible electronics and plasmonics. TCOs are obtained by heavily doping wide-bandgap semiconductors with metal ions; the most common TCOs are Sn-doped In_2O_3 (ITO) and Al-doped ZnO (AZO), where carrier densities exceeding 10^{21} cm^{-3} and resistivities below 10^{-4} Ωcm have been achieved.[8] AZO in particular is gaining great interest as it is an indium-free, low-cost, and easy processable material.[9–12]

The optoelectronic performances of TCOs strictly depend on the quality of the samples and on the growth techniques.[3,8] For example, several experimental measurements[13–16] performed on AZO samples with similar Al contents ($\sim 3\%$) but grown with different methods (e.g. magnetron sputtering, pulsed laser co-ablation, atomic layer, chemical spray or sol-gel deposition), reported a large range of values of the electrical resistivity ($3\times10^{-4} \div 3\times10^{-2}$ Ωcm). A similar variability is reported also for the transparency ratio ($80 \div 90\%$)[17–19] and the injected free charge density ($5\times10^{19} \div 2.0\times10^{21}$ cm^{-3}).[11,15,20]

The discrepancy in these results is usually associated to the presence of defects and impurities in the crystalline host that may act either as scattering centers, which reduce the mobility and the injected charge density, or as optical traps, which absorb light in the visible range. While point and extended defects, such as vacancies and dislocations, have been longly studied for undoped-ZnO, both experimentally[21–24] and theoretically,[25–27] almost nothing is known about the effect of native defects on TCO materials.[28–30] In particular, the relative equilibrium between charge localization and charge compensation in the presence of both point defects and metal dopants is still an unsolved problem.

Here, we present a first principles study of the effect of native oxygen and zinc vacancies and H impurities on the electronic and optical properties of Al-doped ZnO. We demonstrate that oxygen vacancies hardly modify the properties of AZO that are instead very sensitive to Zn vacancies. Furthermore, hydrogen impurities always act as electron donors which increase the free electron density at the bottom of conduction band.

2 Methods

We performed first-principles total-energy-and-forces calculations, based on Density Functional Theory (DFT), as implemented in QUANTUM ESPRESSO.[31] All simulations employed the PBE exchange-correlation functional,[32] a plane

[a] *Istituto Nanoscienze CNR-NANO-S3, I-41125 Modena, Italy.*
[b] *CNR-IMEM, Parco Area delle Scienze, 37A, I-43100 Parma, Italy.*
[c] *Dipartimento di Fisica, Informatica e Matematica, Universitá di Modena e Reggio Emilia, I-41125 Modena, Italy.*
[*] Corresponding author. Fax: +39 059 367488; Tel: +39 059 2055627; E-mail: arrigo.calzolari@nano.cnr.it
† Electronic Supplementary Information (ESI) available: ESI includes accuracy tests on DFT+U approach, the 3D optimized structures described in the text and complementary details on the effects of modification of dopants and defects amount.]. See DOI: 10.1039/b000000x/

View Article Online
DOI: 10.1039/C5TC01699A

wave basis set with a kinetic energy cutoff of 28 Ry (280 Ry) for the wave functions (charge), and ultrasoft pseudopotentials.[33] The DFT bandstructure was corrected by including an *ad hoc* Hubbard potential on both 3*d* orbitals of zinc (U_{Zn}=12.0 eV) and 2*p* orbitals of oxygen (U_O=6.5 eV), along the lines previously described in Ref.[34]. Numerical details and accuracy tests on the effects of the DFT+U approach on the structural and electronic properties of ZnO are reported elsewhere,[34] see also Electronic Supplementary Material (ESI) for further details on the effect of U on AZO (Fig. S1). The AZO bulk crystals were simulated by periodic supercells. We focused on AZO in the sub-solubility limit (Al < 3.5 %), for which the Al ions mainly assume a Zn-substitutional position in the ZnO crystal. AZO cell includes 16 primitive ZnO cells (i.e. 64 atoms), where two non-consecutive Zn atoms were substituted with two Al ions; this corresponds to a formal Al concentration equal to 3.2%. This is the experimental most favorable doping content for TCO applications.[35] Regular grids (4×4×4) of k-points were used for Brillouin zone (BZ) integration. All structures are relaxed until forces on all atoms are lower than 0.03 eV/Å. The 3D relaxed structures are reported in Figure S2 of ESI for completeness.

The electron energy loss (EEL) function is calculated from the complex dielectric function $\hat{\varepsilon}(\omega) = \varepsilon_1 + i\varepsilon_2$, evaluated using the code epsilon.x, also included in the QUANTUM ESPRESSO suite. This code implements an independent particle formulation of the frequency-dependent (ω) Drude-Lorentz model for solids:[7,36]

$$\hat{\varepsilon}(\omega) = 1 - \sum_{\mathbf{k},n} f_{\mathbf{k}}^{n,n} \frac{\omega_p^2}{\omega^2 + i\eta\omega} + \sum_{\mathbf{k},n\neq n'} f_{\mathbf{k}}^{n,n'} \frac{\omega_p^2}{\omega_{\mathbf{k},n,n'}^2 - \omega^2 - i\Gamma\omega}, \quad (1)$$

where ω_p is the bulk plasma frequency; $\hbar\omega_{\mathbf{k},n,n'} = E_{\mathbf{k},n} - E_{\mathbf{k},n'}$ is the vertical band-to-band transition energy between occupied and empty Bloch states, labeled by the quantum numbers $\{\mathbf{k},n\}$ and $\{\mathbf{k},n'\}$, respectively. $f_{\mathbf{k}}^{n,n}$ and $f_{\mathbf{k}}^{n,n'}$ are the oscillator strengths for the Drude and Lorentz parts and are related to the dipole matrix elements between Bloch states.[7,36,37] η, Γ are the Drude-like and Lorentz-like relaxation terms, which account for the finite lifetime of the electronic excitations and implicitly include the effects of the dissipative scattering.[37] In the low-energy range relevant for metals (IR-vis), the adopted value for η (50 meV) corresponds to a dephasing time $\tau = 2\hbar/\eta = 25$ fs, in agreement with the values obtained within the Mie theory for metallic systems.[38] Once the imaginary part of the dielectric function (ε_2) is known, the independent-particle absorption spectra can be straightforwardly obtained using the relation $\alpha(\omega) \propto \omega\varepsilon_2(\omega)$.

The simulation of the color is based on the *tristimulus* colorimetry theory,[39] which provides a red (R), green (G), and blue (B) representation of the perceived hue, starting from the knowledge of an illuminant source (tabulated), the retina matching functions (tabulated)[40] and the absorption spectrum (calculated). The color of a sample can be expressed by three color indexes X, Y, and Z, defined as:[41]

$$\mathrm{XYZ} = N \int I_0(\lambda) \mathrm{e}^{-\alpha(\lambda)\ell} \bar{\mathrm{x}}\bar{\mathrm{y}}\bar{\mathrm{z}}(\lambda) d\lambda, \quad (2)$$

where $\lambda = c/\omega$ is the wavelength, $I_0(\lambda)$ is the incident radiation or *illuminant*. In the present case we used the standard D65 illuminant, which mimics the solar spectrum in the visible range; $\alpha(\lambda)$ is the calculated absorption spectrum; N is a normalization constant and ℓ is the effective thickness traversed by the light beam in the sample. The functions $\bar{\mathrm{x}}\bar{\mathrm{y}}\bar{\mathrm{z}}(\lambda)$ are the *tristimulus* color-matching functions, as defined by the CIE standard (CIE 1931, 2° standard observers[40]). They describe the physiological response of human retina to red, green and blue colors, respectively. When the XYZ values are known, other color representations (*e.g.* RGB or CIELAB) may be trivially obtained through linear transformations.

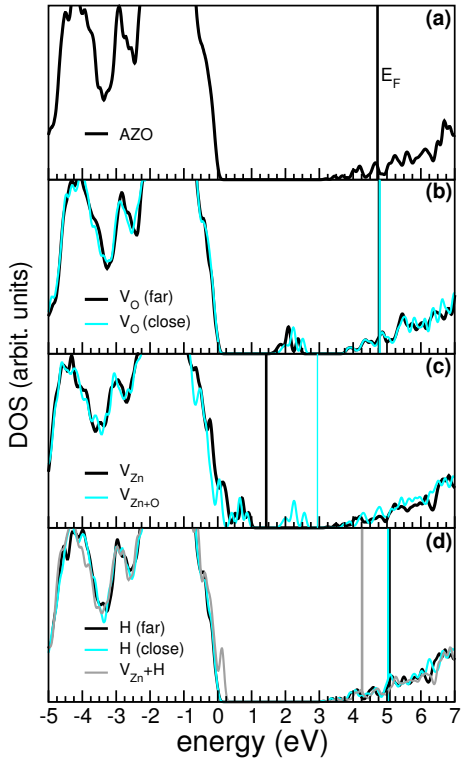

Fig. 1 Total DOSs of AZO bulk in the presence of (a) no defects, (b) oxygen vacancies (V_O), (c) zinc (V_{Zn}) and zinc-oxygen dimer (V_{Zn+O}) vacancies, (d) hydrogen impurities. Vertical lines mark the Fermi level of each system. Zero energy reference is set to ZnO valence band top.

View Article Online
DOI: 10.1039/C5TC01699A

3 Results and Discussion

Starting from the undefective AZO crystal taken as a reference, we studied three sets of systems: (i) neutral oxygen vacancies (V_O), (ii) zinc and zinc-oxygen dimer vacancy (V_{Zn} and V_{Zn+O}, respectively); and (iii) hydrogen impurities (H). Two different structures were considered for the case of oxygen vacancies: in one case (labeled *far*) the oxygen is removed from the ZnO host far away from the Al impurity, in the other (labeled *close*) the removed oxygen would be bonded to aluminum; in the former case the Al ion is tetra-coordinated, in the latter it is ter-coordinated with next-neighbor oxygens. In the Zn-substitutional configuration, Al has not Zn as first-neighbor, thus for V_{Zn} and V_{Zn+O} cases we considered only one geometry, equivalent to the *far* configuration of V_O. Experimental results[42,43] indicate that the hydrogen penetrates in ZnO in the dissociated (atomic) form and adsorbs to oxygen in an interstitial position, we therefore considered two possible hydrogen adsorption sites, one *far* and *close* Al, as for the V_O case.

The results of the electronic structure calculation for fully optimized structures are reported in Figure 1. Undefective AZO (panel a) has the typical character of highly degenerate *n*-type conductor: Al fully donates its $3p$ electron to ZnO, partially filling the bottom of the host conduction band, without inserting any defect state in the gap, nor changing the effective mass of ZnO.[7,10] The presence of V_O (panel b) does not change this picture: V_O is a deep defect, which introduces fully occupied states in the gap, in agreement with previous theoretical and experimental data for un-doped ZnO.[44,45] However, this does not modify the transport properties of AZO, which maintains its *n*-degenerate conductive behavior. Even though the *far* vacancy results to be energetically more stable than the *close* one by ~ 1.1 eV, from the electronic point of view the two configurations are almost identical. The final position of the Fermi level also coincides with the AZO case, implying a same amount of injected free electron charge (see below). Rather, the exact position of the Fermi level is strictly dependent on the amount of doping amount. In Figure S3 of ESI, we compare the DOS plots of both V_O *far* and *close* systems evaluated at 1.6% and 3.2 % of Al content, respectively: The only observed effect of the reduced dopant dosage is a shift of the Fermi level towards the bottom of the conduction band (i.e. lower free electron charge), as expected for intrinsic conductors.

On the contrary, Zn vacancy is a dominant acceptor in ZnO (panel c): the removal of a Zn atom in ZnO induces a net depletion of charge, leaving the four first-neighbor oxygens under-coordinated. This introduces shallow defect states close to the valence band top of the pristine ZnO.[21,24] The inclusion of two Al donors just saturates the V_{Zn} electron unbalance, but it is not sufficient to transfer charge into the conduction band.

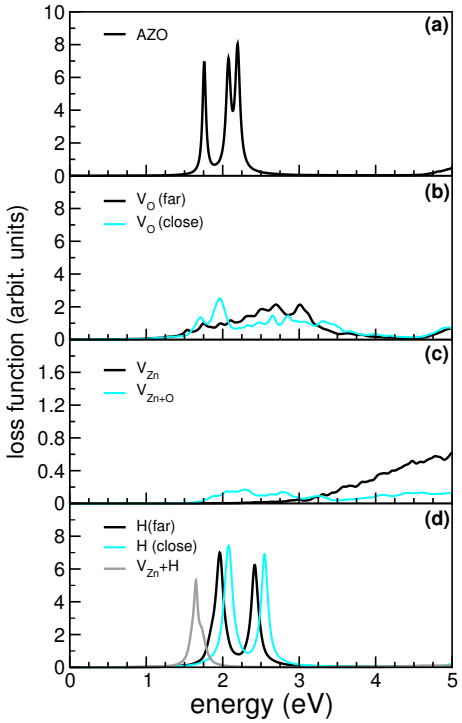

Fig. 2 Electron energy loss spectra of AZO bulk in the presence of (a) no defects, (b) oxygen vacancies (V_O), (c) zinc (V_{Zn}) and zinc-oxygen dimer (V_{Zn+O}) vacancies, (d) hydrogen impurities.

As a consequence, the system has a semiconducting character, with the Fermi level lying within the gap, i.e. the presence of V_{Zn} strongly perturbs the TCO behavior of AZO.

This balance is rigorously true for the present ratio (1:2) between the V_{Zn} and Al content, i.e. where the p electrons of the two Al ions in the cell exactly compensate the removal of the two s electrons associated to one Zn vacancy. In general, the final electrical character of a real sample would depend on this ratio: for controlled-growth materials with a low percentage of intrinsic defects, Al doping compensates the electron withdrawing of zinc vacancies, imparting a conducting behavior to the system, albeit with reduced electron densities with respect to the ideal AZO case. On the contrary for highly defective samples, the electron-acceptor effect of V_{Zn} dominates canceling the Al contribution to *n*-doping, restoring a compensated semiconductor material. To demonstrate this statement in Figure S4 of ESI we report the DOS plots of AZO materials with different Al and V_{Zn} amounts. We first considered a formal doping equal to 1.6%, where we kept fixed the Zn vacancy-dopant ratio (1:2). In this case the picture remains qualitatively the same, and the systems maintains a semiconducting behavior as in Figure 2c. Different are instead the cases where the Zn vacancy-dopant ratio is altered, keeping

View Article Online
DOI: 10.1039/C5TC01699A

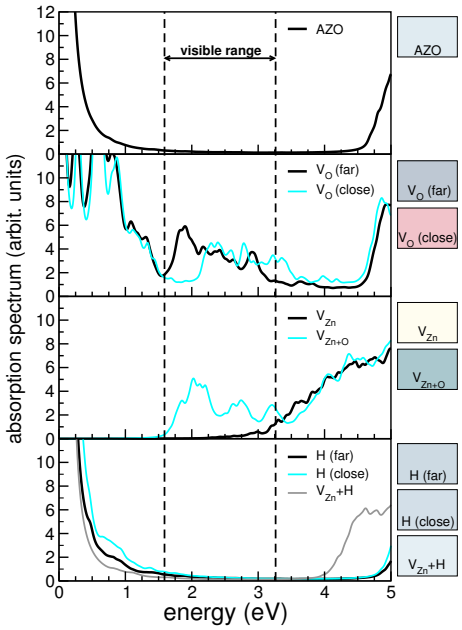

Fig. 3 Absorption spectra of AZO bulk in the presence of (a) no defects, (b) oxygen vacancies (V_O), (c) zinc (V_{Zn}) and zinc-oxygen dimer (V_{Zn+O}) vacancies, (d) hydrogen impurities. Vertical dashed lines defines the visible range. Lateral boxes represent the simulated colors corresponding to each system.

fixed the formal doping dosage (3.2 %). When the number of vacancy exceeds this ratio (e.g. 3:4) the Fermi moves towards the top valence band, when the opposite is realized (e.g. 1:4) the amount of free charge provided by the Al dopant is able to restore the n-type behavior of the undefective AZO material. Thus, the modification of the compensation ratio radically modifies the electrical character of the system that results semiconducting in vacancy rich conditions while it gives back the intrinsic TCO behavior of undefective AZO in Al rich conditions. This wide range of possibilities shed light on the plethora of contrasting experimental results, ideally collected at the same formal doping amount.[13–16]

The removal of a Zn-O dimer (V_{Zn+O}) is nothing but the combination of the single atom vacancies. In panel c, we identify both the deep (occupied) levels introduced by the absence of the O atom and the shallow level due to Zn vacancy. As in the previous case, the Zn vacancy is the dominant feature, which perturbs the conducting character of AZO.

Hydrogen impurity is considered the main responsible for the unintentional *n*-type doping in ZnO. When added to AZO (panel d) H maintains its donor activity, increasing the amount of free electron density in ZnO conduction band (note the blue-shift of the Fermi level with respect to AZO). From Figure1 it is also evident that the doping effect of H is not related to the adsorption position with respect to aluminum. The two structures also result almost degenerate in energy ($\Delta E \approx 15$ meV). The combination of V_{Zn} and H impurities restores the typical *n*-type conducting behavior to AZO, with a reduction of the injected charge (note the red-shift of the Fermi level with respect to undefective AZO). This confirms also the role of charge compensation effects in the presence of Zn vacancies.

In order to quantify the effects of defects on charge injection, we calculated the electron energy loss function. We first evaluated the complex dielectric function $\hat{\varepsilon}(\omega)$, then the electron energy loss function can be easily obtained as $L(\omega) = Im\{-1/\hat{\varepsilon}\}$. When both the imaginary and real part of the dielectric function are zero, $L(\omega)$ has a peak that corresponds to the plasma frequency ω_p of the system (Figure 2). The plasma frequency lies in the UV region for intrinsic ZnO, while it is in the visible range for native AZO. This makes AZO an efficient plasmonic material in the near-IR/visible range.[6,7,12] The multi-peak structure of panel (a) is related to long-range Al-Al interaction due to the high doping level.[7] By inverting the Drude definition of the plasma frequency $\omega_p = \sqrt{\frac{e^2 n_e}{\varepsilon_0 m_e^*}}$ (where e is the electron charge, ε_0 the dielectric permittivity of vacuum and m_e^* the electron effective mass), we can extract the free electron density n_e. For AZO we obtain $n_e = 8.7 \times 10^{20}$ cm^{-3}. Very similar is the case of oxygen vacancies (panel b) for which the calculated free electron density is $\sim 8.1 \times 10^{20}$ cm^{-3} for both configurations. The broadening of loss function in the visible range is related instead to interband optical transitions between the deep gap states and the conduction band. Thus, even though the oxygen vacancies hardly modify the electrical properties of AZO, they affect the optical properties, i.e. the transparency of the material (see below).

In agreement with the description of the electronic structure, the presence of zinc vacancies (panel c) induces a semiconducting behavior to the system that do not exhibit anymore a plasma-like feature in the IR-visible range (note the difference in the y-axis scale). The edge of the $L(\omega)$ function at ~ 3.0 eV (black curve) corresponds to the optical valence-to-conduction band of ZnO. The optical gap is reduced to 1.9 eV in the V_{Zn+O} case, because of the in-gap states associated to the oxygen vacancy. The electron donation of H defects is confirmed by the loss function (panel d) and the calculated charge density is $n_e \sim 1.2 \times 10^{21}$ cm^{-3} for both configurations. The co-existence of V_{Zn} and H impurities gives rise to a plasma frequency in the visible range, but at lower frequency, which corresponds to a lower charge injection $n_e = 5.7 \times 10^{20}$ cm^{-3}. The charge redistribution in this case, which completely removes residual charge from Al sites, washes out the internal structure of the plasmonic peak.

According to the semiclassical picture provided by the Maxwell equations, the absorption coefficient $\alpha(\omega)$ can be

View Article Online
DOI: 10.1039/C5TC01699A

written in terms of the imaginary part (ε_2) of the complex dielectric function: $\alpha(\omega) \propto \omega\varepsilon_2(\omega)$. The results for independent-particle and dipole approximation[46] are summarized in Figure 3, where we also delimited the visible range between two dashed vertical lines. In agreement with the experimental results,[17,18] AZO absorbs very weakly in the visible range resulting almost, but not completely, transparent. The residual absorption is related to the Al-filled conduction band states. As the color is associated to the transmitted (i.e. not-absorbed) radiation, the absorption in the lower energy range (red region) imparts a very light navy-blue hue to AZO (Fig. 3, right). Infrared and lower energy absorption is associated to the *dc*-conductivity of metallic systems.

The deep gap states induced by the oxygen vacancies, while not perturbing the electrical properties, are optically active and absorb light in the visible range. This further reduces the transparency of the sample, as elucidated also by the darker simulated colors (panel b). The small differences in the absorption spectra are more evident in the simulated colors, as the eye-sensitivity to red, green, and blue is not linear in the visible range.[39] Thus, the hypsochromic shift of V_O (*close*) spectrum results in a reddish coloration. V_{Zn}-AZO has the typical wide-bandgap semiconducting behavior dominated by interband transitions in the UV range, this corresponds to an almost perfect transparent sample, as the undoped ZnO crystal. The presence of O-derived states in V_{Zn+O} system increases the absorption in the visible range, reducing the transparency. The absorption spectra in the presence of H result very similar to pristine AZO one, the corresponding color is slightly darker because of the increased free electron DOS at the bottom of the conduction band.

4 Conclusions

Our first principles results describe the effects of native point defects on the optical and electronic properties of Al-doped ZnO. In particular, we show that O-vacancies do not affect conductivity although reducing transparency, while Zn vacancies may destroy the TCO behavior. We finally demonstrate that H impurities, often present in experimental samples, not only passivate defects and dangling bonds, but also improve the TCO performances, donating extra free charge also in presence of Zn or O vacancies.

From one side, the chemistry and the density of defects are strictly dependent on growth techniques and on growth conditions (e.g. temperature, pressure, deposition time, etc); on the other side the type of defects (e.g. oxygen vs zinc vacancies) selectively affects the electrical or optical properties of the materials. Thus, the engineering of native defects along with the control of the compensation effects, via the proper choice of the experimental setup, can be an implemented step to optimize either the conduction or the transparency of TCO systems: this is particularly true for low-dimensional structures, such as wires, tetrapods and nanoparticles, where vacancies are most frequent.[19,24,47]

References

1 J. E. Medvedeva and C. L. Hettiarachchi, *Phys. Rev. B*, 2012, **81**, 125116 (1–16).
2 J. L. Castañeda, *Mater. Sci. Appl.*, 2010, **2**, 1233–1242.
3 A. Stadler, *Materials*, 2012, **5**, 661–683.
4 C. G. Granqvist, *Sol. Energy Mater. Sol. Cells*, 2007, **91**, 1529–1598.
5 K. Ellmer, *Nature Photonics*, 2012, **6**, 809–817.
6 G. V. Naik, V. M. Shalaev and A. Boltasseva, *Adv. Mater.*, 2013, **25**, 3264–3294.
7 A. Calzolari, A. Ruini and A. Catellani, *ACS Photonics*, 2014, **1**, 703–709.
8 P. D. C. King and T. D. Veal, *J. Phys. Condens. Matter.* , 2011, **23**, 334214 (1–17).
9 H. Kim, C. M. Gilmore, J. S. Horwitz, H. M. A. Piqué, G. P. Kushto, R. Schlaf, Z. H. Kafafi and D. B. Chrisey, *Appl. Phys. Lett.* , 2000, **76**, 259–261.
10 M. Bazzani, A. Neroni, A. Calzolari and A. Catellani, *Appl. Phys. Lett.* , 2011, **98**, 121907 (1–3).
11 E. Sachet, M. D. Losego, J. Guske, S. Franzen and J.-P. Maria, *Appl. Phys. Lett.* , 2013, **102**, 051111 (1–3).
12 A. K. Pradhan, T. Holloway, R. Mundle, H. Dondapati and M. Bahoura, *Appl. Phys. Lett.* , 2012, **100**, 061127 (1–3).
13 Y.-Y. Chen, J.-C. Hsu, P. W. Wang, Y.-W. Pai, C.-Y. Wu and Y.-H. Lin, *Appl. Surf. Sci.*, 2011, **257**, 3446–3450.
14 H. Kim, M. Osofsky, S. M. Prokes, O. J. Glembocki and A. Piqué, *Appl. Phys. Lett.* , 2013, **102**, 171103 (1–3).
15 D. Guo, K. Sato, S. Hibino, T. Takeuchi, H. Bessho and K. Kato, *J. Mater. Sci.*, 2014, **49**, 4722–4734.
16 C. Liu, Z. Xu, Y. Zhang, J. Fu, S. Zang and Y. Zuo, *Mater. Lett.*, 2015, **139**, 279–283.
17 S. Tabassum, E. Yamasue, H. Okumura and K. N. Ishihara, *J. Mater. Sci.- Mater. Electronics*, 2014, **25**, 4883–4888.
18 A. Monemdjou, F. E. Ghodsi and J. Mazloom, *Superlatt. Microstr.*, 2014, **74**, 19–33.
19 E. Della Gaspera, A. S. R. Chesman, J. van Embden and J. J. Jasieniak, *ACS Nano*, 2014, **8**, 91549163.
20 Q. You, P. Liang, Y. Li, H. Cai, X. Yang, F. Huang, J. Sun, N. Xu and J. Wu, *Mater. Lett.*, 2015, **139**, 228–231.
21 D. C. Look, G. C. Farlow, P. Reunchan, S. Limpijumnong, S. B. Zhang and K. Nordlund, *Phys. Rev. Lett.* , 2005, **95**, 225502 (1–4).
22 L. Schmidt-Mende and J. L. MacManus-Driscoll, *Mater. Today*, 2007, **10**, 40–48.

View Article Online
DOI: 10.1039/C5TC01699A

23 M. D. McCluskey and S. J. Jokela, *J. Appl. Phys.*, 2009, **106**, 071101 (1–13).

24 F. Fabbri, M. Villani, A. Catellani, A. Calzolari, G. C. Cicero, D. Calestani, G. Calestani, A. Zappettini, B. Dierre and T. Sekiguchi, *Sci. Rep.*, 2014, **4**, 5158 (1–7).

25 S. Lany and A. Zunger, *Phys. Rev. Lett.* , 2007, **98**, 045501 (1–4).

26 A. F. Kohan, G. Ceder, D. Morgan and C. G. Van de Walle, *Phys. Rev. B*, 2006, **61**, 15019–15027.

27 P. Erhart, K. Albe and A. Klein, *Phys. Rev. B*, 2006, **73**, 205203 (1–9).

28 J. H. Noh, H. S. Jung, J.-K. Kim, C. M. Cho, J.-S. An and K. S. Hong, *J. Appl. Phys.* , 2008, **104**, 073706 (1–5).

29 B. Li, Y. Adachi, J. Li, H. Okushi, I. Sakaguchi, S. Ueda, H. Yoshikawa, Y. Yamashita, S. Senju, K. Kobayashi, M. Sumiya, H. Haneda and N. Ohashi, *Appl. Phys. Lett.* , 2011, **98**, 082101 (1–3).

30 Q. Jiang, W. Wang, Y. Zeng, W. Xu, J. Huang, T. Zhou and W. Song, *J. Mater. Sci.: Mater. Electron.*, 2014, **25**, 5356–5361.

31 Giannozzi, P.; Baroni, S.; Bonini, N.; Calandra, M.; Car, R.; Cavazzoni, C.; Ceresoli, D.; Chiarotti, G. L.; Cococcioni, M.; Dabo, I.; Dal Corso, A.; de Gironcoli, S.; Fabris, S.; Fratesi, G.; Gebauer, R.; Gerstmann, U.; Gougoussis, C.; Kokalj, A.; Lazzeri, M.; Martin-Samos, L.; Marzari, N.; Mauri, F.; Mazzarello, R.; Paolini, S.; Pasquarello, A.; Paulatto, L.; Sbraccia, C.; Scandolo, S.; Sclauzero, G.; Seitsonen, A. P.; Smogunov, A.; Umari, P.; Wentzcovitch, R. M. *J. Phys.: Condens. Matter* **2009** *21*, 395502. See also `www.quantum-espresso.org`.

32 J. P. Perdew, K. Burke and M. Ernzerhof, *Phys. Rev. Lett.* , 1996, **77**, 3865–3868.

33 D. Vanderbilt, *Phys. Rev. B*, 1990, **41**, R7892–R7895.

34 A. Calzolari, A. Ruini and A. Catellani, *J. Am. Chem. Soc.* , 2011, **133**, 5893–5899.

35 H. Mondragón-Suárez, A. Maldonado, M. de la L Olvera, A. Reyesb, R. Castanedo-Pérez, G. Torres-Delgadoc and R. Asomoza, *Appl. Surf. Sci.*, 2002, **193**, 52–59.

36 R. Colle, P. Parruccini, A. Benassi and C. Cavazzoni, *J. Phys. Chem. B*, 2007, **111**, 2800–2805.

37 Wooten, F. *Optical Properties of solids*, **1972** Academic Press, Inc. San Diego CA, 9211 USA.

38 Aeschlimann, M. Electron Dynamics in Metallic Nanoparticles in *Encyclopedia of Nanoscience and Nanotechnology*, Ed. by Nalwa N. **2004** American Scientific Publishers, USA.

39 Ohtha, N.; Robertson, A. R. *Colorimetry: Fundamentals and applications*, John Wiley & Sons Ltd UK (2005.).

40 http://en.wikipedia.org/wiki/CIE_1931_color_space.

41 O. B. Malcıoğlu, A. Calzolari, R. Gebauer, D. Varsano and S. Baroni, *J. Am. Chem. Soc.*, 2011, **133**, 15425–15433.

42 H. Qiu, B. Meyer, Y. Wang and C. Wöll, *Phys. Rev. Lett.* , 2008, **101**, 236401 (1–4).

43 F. Traeger, M. Kauer, C. Wöll, D. Rogalla and H.-W. Becker, *Phys. Rev. B*, 2011, **84**, 075462 (1–10).

44 B. Lin, Z. Fu and Y. Jia, *Appl. Phys. Lett.* , 2001, **79**, 943–945.

45 A. Janotti and C. G. Van de Walle, *Phys. Rev. B*, 2007, **76**, 165202 (1–22).

46 The present method does not include many-body excitonic effects. While sizeable exciton binding energies were observed for metal-oxide based wide-gap materials (such as defective MgO[?]), excitonic effects are known to be minor for metallic systems - like most of the here considered defective AZO samples - due to the enhanced screening in the direct electron-hole Coulomb interaction.

47 X. Tang, E. S. Guang-Choo, L. Li, J. Ding and J. Xue, *Chem. Mater.*, 2010, **22**, 33833388.

View Article Online
DOI: 10.1039/C5TC01699A

Graphical Abstract for: "Optoelectronic properties and color chemistry of native point defects in Al:ZnO transparent conductive oxide", by A. Catellani, A. Ruini and A. Catellani

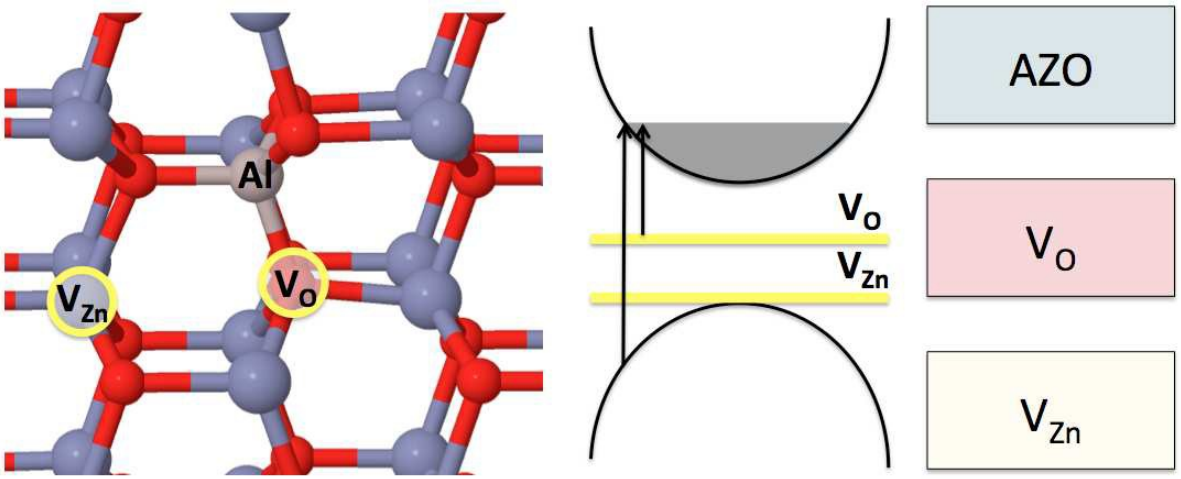

The effects of native defects (e.g. V_O, V_{Zn}, H) on the TCO properties and color of Al:ZnO (AZO) material are investigated by using first principles calculations.